Rev.Adv.Mater.Sci. 6 (2004) 23-31

3-DIMENSIONAL WULFF DIAGRAMS FOR Σ3 GRAIN BOUNDARIES IN Cu

B. Straumal[1], Ya. Kucherinenko[2] and B. Baretzky[3]

[1]Institute of Solid State Physics, Russian Academy of Sciences, Chernogolovka, Moscow distr., 142432 Russia,
[2]Geological faculty, Moscow Lomonosov State University, Vorobjovy gory, 119992 Moscow, Russia
[3]Max-Planck-Institut für Metallforschung, Heisenbergstrasse 3, D-70569 Stuttgart, Germany

Received: May 15, 2004

Abstract. The faceting of cylindric tilt grain boundary in Cu bicrystal containing full spectrum of inclinations has been studied at 0.95 of melting temperature T_m. Both grains form the superlattice called coincidence site lattice (CSL) with Σ=3. The $(100)_{CSL}$ facet and non-CSL 82°9*R* facet are observed. The ratio between GB energy σ_{GB} and surface energy σ_{sur} was measured by atomic force microscopy using the GB thermal groove method. The influence of misorientation deviation $\Delta\theta = |\theta - \theta_{\Sigma}|$ from coincidence misorientation θ_{Σ} has been studied. The 3-dimensional Wulff-Herring diagrams were constructed using measured σ_{GB}/σ_{sur} values. They reveal that only $(100)_{CSL}$ and 9*R* facets correspond to the energy minimum at low Dq. No rough edges between $(100)_{CSL}$ and 9*R* facets were observed. It means that T_m is lower than the roughening temperature for these facets in Cu. With increase of $\Delta\theta$, the energy of $(100)_{CSL}$ facet increases.

1. INTRODUCTION

In the case of ordinary coexistence of two bulk phases a large inclusion of one phase may remain in stable equilibrium inside of the second phase (matrix). The average shape of the inclusion is then determined by strictly thermodynamic considerations based on the free energy minimum for the creation of necessary interfacial boundary [1, 2]. If both coexisting phases are isotropic *(e.g*. fluids), the shape of the inclusion is spherical. If one or both are crystalline or otherwise anisotropic, interfaces of some orientations are preferred over those of the other orientations, and the "equilibrium crystal shape" (ECS) of the inclusion is nonspherical and may be more or less complex. The problem of ECS was first considered by Wulff [3, 4]. He proposed the following construction (see. Fig. 1). When interface free energy per unit area *f*(***m***) is drawn as a polar plot (Wulff plot sometimes called γ-plot), the crystal shape is given as the interior envelope of the family of perpendicular planes passing through the end of radius-vectors ***m*** *f*, where ***m*** is the unit outward normal to the interface. Such crystal shape corresponds to the minimum of the free energy. Andreev [5] following the approach of Landau [6] first pointed out in this context that the Wulff construction is simply the geometrical version of a two-dimensional Legendre transformation between the free energy *f*(***m***) and the crystal shape *r*(***h***). ***h*** is the facet orientation relative to crystal axes. It means that knowing the *f*(***m***) energy one can reconstruct the equilibrium crystal shape and vise versa *r*(***h***).

Two limiting cases of ECS are completely faceted shapes (polyhedra), consisting entirely of strictly planar faces (facets) joined at sharp edges, and completely rounded shapes, which are smoothly curved everywhere and lack both facets and edges. It is generally supposed that macroscopic equilibrium crystals at temperature $T = 0$ are completely faceted (polyhedral). However, at nonzero temperatures curved interfacial regions may appear in addition to planar facets [2]. The theoretical picture of the thermal evolution of the equilibrium crystal shape (ECS) of a typical crystal [1, 2, 7, 8]. As *T* increases,

Corresponding author: B.B. Straumal, e-mail: straumal@issp.ac.ru

facets shrink and eventually disappear [1] each facet at its own characteristic roughening ("faceting") temperature $T_R(\boldsymbol{h})$ [7]. At sufficiently high temperature the ECS becomes everywhere smoothly rounded (unless, of course, the system first undergoes a bulk phase change, such as melting). In [2] the ECS for crystals with cubic lattice were calculated for a three-dimensional ferromagnetic Ising model with both nearest-neighbor (J_1) and next-nearest-neighbor ($J_2 = R J_1$) interactions at nonzero temperatures. If $R > 0$ the {100} facet first appear by decreasing temperature at completely rounded surface. At lower temperatures facets {110} and than {111} facets have to appear one after another, also at rounded parts of the surface. This scenario seems consistent with the present experimental situation for surfaces, although the difficulty of achieving equilibrium on a laboratory-feasible time scale imposes severe restrictions on the ranges of crystal size and temperature which can be investigated. The experiments with small droplets of pure Au reveal the presence of {100} and {111} facets at $T = 0.94\ T_m$ (T_m being the melting temperature) [9]. Similar measurements with Pb droplets in the temperature interval from 0.78 to 0.96 T_m demonstrated the presence of {100} and {111} facets [10]. These facets were separated by smooth regions, facets shrink with increasing temperature, and facet {100} almost disappears. The hcp ^{4}He was the first system which has been studied through a sequence of three faceting/roughening transitions at T_R = 1.3, 1.0 and 0.4K into the everywhere-rounded regime [11, 12]. The *in-situ* observation of growth of ^{3}He crystals from the superfluid phase permitted to reveal three roughening transitions in sequence T_R (110) = 0.26-0.34K, T_R (100) = 0.13-0.17K and T_R (211) = 0.087-0.113K [13].

When ECS contains both rounded and faceted regions joined at edges, these edges may be either 'sharp' (slope discontinuity) or 'smooth' (no slope discontinuity). Both sharp and smooth edges have been seen in experiments, respectively in Au [11] and Pb [12, 14]. Conventional phase boundaries are the loci of nonanalyticity of a free-energy surface, i.e., the set of values of its arguments at which the free energy is singular. The loci $\boldsymbol{h}(T)$, or $T(\boldsymbol{h})$, of nonanalyticity of the crystal-shape function $r(\boldsymbol{h}, T)$ are the crystal edges. Thus, if the crystal shape is to be regarded as a free energy, then, correspondingly, the crystal edges should be regarded as phase boundaries. Thermodynamically, one distinguishes between first-order phase boundaries, characterized by discontinuities in one or more first derivatives of the free energy, and second-order phase boundaries, characterized by continuous first derivatives. For crystal shapes, this distinction is between the sharp edges (as seen for the gold crystals) and the smooth edges (as seen for the lead crystals). The behavior of a free energy in the near vicinity of a second-order phase transition is characterized by critical singularities, often of power-law type. Therefore, the shape of a crystal surface near a smooth edge is described by a power law with an exponent λ. λ was measured experimentally for Pb ($\lambda = 1.60 \pm 0.15$ [14]) and ^{4}He ($\lambda = 1.55 \pm 0.06$ [15]). It is very close to the critical exponent $\lambda = 3/2$ for the so-called Pokrovsky-Talapov universality class [16].

Later the more complicated phenomena of ECS were observed both experimentally and theoretically. Particularly, the coupled compositional and roughening phase transitions in Pb-based alloys were found [17], the values for the absolute step and kink energies for lead and other metals [18–23], Si [24, 25] and TiN [26, 27] were obtained, the deviation of λ from Pokrovsky-Talapov behaviour was observed [28]. The tricriticality in the orientational phase diagram of Si (113) surface misoriented towards [001] has been explained by the attractive step-step interaction [29, 30]. Big variety of possible behavior of facet ridge end points in crystal shapes was predicted recently with the aid of body-centered solid-on-solid model with an enhanced uniaxial interaction range [31].

However, up to now mainly the situation was considered both theoretically and experimentally when only one phase (namely the 'inclusion') is anisotropic and the second phase is isotropic (gas, liquid). It corresponds to the case of outer surface of crystals. What happens when both 'matrix' and 'inclusion' are crystalline and, therefore, anisotropic? Grain boundaries being the interfaces between two identical but misoriented lattices represent the simplest case. Evidently, one important condition is not valid for grain boundaries (GBs), namely the volume of 'inclusion' is not constant, and the problem of ECS for isolated GB is similar to those of slowly growing of slowly diluting crystal. However, this small trouble is completely compensated by the rich variety of possible crystallographic features of GBs. The ECS of isolated grain is governed by the strong interaction between two crystal lattices L_1 and L_2 of both grains. At certain misorientations Ψ_Σ some sites in lattices L_1 and L_2 coincide forming the superlattice called coincidence site lattice (CSL) [32, 33]. CSL is characterized by the reciprocal density of coinciding sites Σ. The close-packed planes in CSL play for GBs the role similar to that of

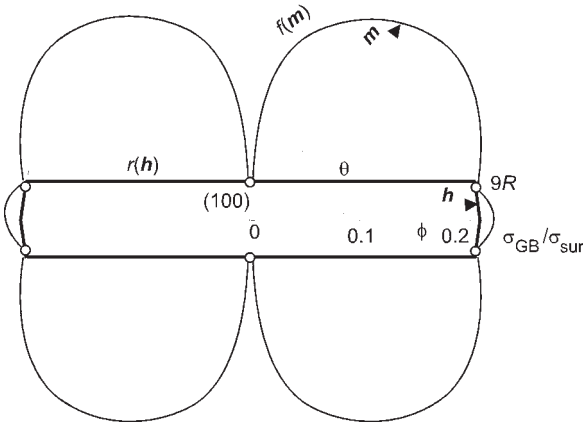

Fig. 1. Wulff diagram for the Σ3 Cu tilt GBs with exact coincidence. ϕ and ϕ are angular variables which measure interfacial orientation (***m***) and crystal shape (***h***), respectively.

close-packed crystal planes for the surfaces. The height of an elementary step at the close-packed CSL planes and the length of the Burgers vector of intrinsic GB dislocations are defined by the displacement shift complete lattice (DSÑ) [34]. DSC is the inverse lattice for CSL in cubic crystals. The height of an elementary step at the less close-packed CSL planes is defined by the so-called grain boundary shifts lattice (GBSL) [35, 36]. It has been shown that GBs possess special structure and properties (including faceting) in certain angular interval $\Delta\Psi$ close to the coincidence misorientations Ψ_Σ and below certain temperature $T_C(\Sigma)$. T_C decrease linearly with increasing Σ and exponentially with increasing $\Delta\Psi$ [37]. It has been supposed that this phenomenon is governed by the GB roughening transition of Pokrovsky-Talapov type [37, 38].

The low-Σ grain boundaries (GBs), Σ being the inverse density of coincidence sites, and their faceting play a very important role in the GB engineering, especially in nanocrystalline materials. Particularly, it has been observed that the number of faceted GBs decrease with increasing temperature in various materials like alumina [39], stainless steel [40], silver [41] and nickel-based superalloys [42]. The presence of GB faceting correlates in these materials with the phenomenon of abnormal grain growth. Above certain temperature the faceted GBs are absent and the abnormal grain growth does not appear [39–43]. The influence of the GB faceting is not occasional, since only so-called special GBs with misorientation angle θ close to the coincidence misorientation θ_Σ can facet. Special GBs exist in certain areas of q and temperature. Particularly, the maximal temperature where GBs possess their special structure and properties decreases with increasing Σ [37]. It means that with decreasing temperature the number if special GBs increases, and the total angular interval for GBs able to facet increases as well. On the other hand, it has been observed that in certain materials the number of low-Σ GBs is surprisingly high [44–47]. The number of low-Σ GBs, exceeds the theoretical value for a random polycrystal, derived by Mackenzie [48, 49]. Particularly the frequency of Σ3 GBs in Ni can reach almost 30% in Ni in comparison with Mackenzie value of 6 to 8 % [44]. It has been demonstrated that the production method, mechanical or thermal treatment, as well as annealing in magnetic field can influence the occurrence frequency of low-Σ and particular that of Σ3 GBs [39, 44, 50, 47]. The high number of Σ3 GBs in polycrystals can be explained by the very broad angular interval $\Delta\theta = |\theta - \theta_\Sigma|$ where Σ3 GBs possess their special structure and properties. The data on GB energy measurements in Al and NiO and on the structural investigations in Al, Pb and Au deliver the value of as high as 10 to 20° [51–57]. Therefore, the investigation of faceting of Σ3 GBs is so important for the GB engineering.

The most natural way to describe the ECS of GB and its evolution is the construction of Wulff diagrams. However, the traditionally used two-dimensional Wulff diagrams are not sufficient for the description of multidimensional space which includes all GB crystallographic parameters. In this work the approach is developed for the construction of 3-dimensional Wulff diagrams. It has been used for the Σ3 twin GBs in Cu.

2. EXPERIMENTAL

For the investigation of GB faceting, a cylindrical Cu bicrystal with an island grain was grown by the Bridgman technique [58] from Cu of 99.999 wt.% purity. The interior grain *1* in this bicrystal is surrounded by the exterior grain *2* forming the Σ9 <110> tilt GB. The $\{111\}_1/\{115\}_2$ or $(110)_{\Sigma 9CSL}$ inclination of S9 GB is unstable against the dissociation reaction: $\Sigma 9 \rightarrow \Sigma 3 + \Sigma 3$ (the subscripts 1 and 2 correspond to the grains *1* and *2*). Therefore, twins (Fig. 2) characterized by well developed Σ3 GBs ?appear during the growth of bicrystal instead of $\{111\}_1/\{115\}_2$ or $(110)_{\Sigma 9CSL}$ facets [59]. The section of Σ3 CSL perpendicular to the {110} tilt axis with position of $(100)_{CSL}$ and 9R facets is shown in Fig. 2a. On the other hand, a natural spread in misorientation

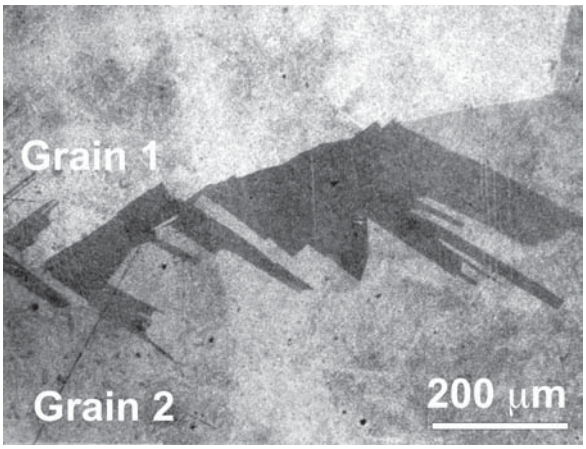

Fig. 2. Micrograph of multiple twins between grain *1* and grain *2* with Σ9 misorientation. Common [110] axis is perpendicular to the micrograph plane.

angle θ of Σ3 twin GBs is present in the bicrystal. Two reasons lead to the appearance of this spread. Firstly, the bicrystals grown by the Bridgman technique are not completely ideal. The cells misoriented in low-angles are always present in the single- and bycrystals due to the instability of growth process. Secondly, the misorientation between seeds *1* and *2* is not exactly Σ9. The multiple twin embrions appear during growth in different locations of $(110)_{\Sigma 9CSL}$ facets leading to the q spread. Since GB energy and q can be measured rather exact and very locally, this natural spread (about 1°) was used to investigate the misorientation influence on the GB faceting of Σ3 twin GBs.

2.5 mm thick platelets were cut from the grown bycrystal perpendicularly to the growth axis. The platelets were ground with 4000 SiC paper and polished with 3 and 1 μm diamond paste. After that they were annealed in 80% Ar + 20% H_2 gas mixture (purity of gases is 99.999%) at pressure of $2 \cdot 10^4$ Pa at different temperatures 1293K, 48 h. During the annealing the GB migrates slowly (10^{-10}–10^{-13} m/s) under the action of capillary driving force. The GB migration permits the facets to develop which are in equilibrium at the respective annealing temperature. The annealed samples were than etched in the 50% HNO_3 aqueous solution. The GB shape was photographed in polarized light in bright and dark field with the aid of an Zeiss Axiophot optical microscope. The sample annealed at 1293K was then carefully repolished and annealed 48 h once again in order to form GB thermal grooves. The profiles of the formed GB thermal groove were analysed with the aid of the Topometrix 2000 Explorer atomic force microscope (AFM) operating in the contact mode. The typical field analyzed with the aid of AFM had a dimension 50´50 mm containing 500´500 pixels. For the analysis, each 10 neighbouring profiles were used to obtain a mean GB groove profile. The ratio between GB energy σ_{GB} and surface energy σ_{sur} was calculated from the relation $\sigma_{GB} = 2\sigma_{sur}\cos(\alpha/2)$ using the values of measured GB groove angles a [60]. For the determination of the groove angle not only the groove tip but the full groove profile was used [61]. Two sides of the groove profile were approximated separately beginning from the maximum on the groove profile. As it was demonstrated previously, the finite radius of the AFM needle does not allow to measure correctly the profile close to the tip of the groove [60, 61]. Therefore, the approximated 'left' and 'right' halves of the groove profile were extrapolated down to their intersection point. This procedure allows to determine the coordinates of the 'true' groove tip which is positioned lower than the tip observed by the AFM. Local misorientation was determined in the same locations as GB energy by scanning electron microscopy (SEM) with the aid of electron backscattering diffraction patterns (EBSD). The orientation was determined with a commercially available system (OIM™, by TSL) capable of automatic pattern indexing. The accuracy in misorientation determination was about 0.5°.

3. RESULTS AND DISCUSSION

At T = 1293K = 0.95 T_m (i.e. very close to the melting temperature) Σ3 GB contains two facets. The scheme for crystallography of both facets is shown in Fig. 3a. The energy of symmetric Σ3 twin ($\{111\}_1$/$\{111\}_2$ or $(100)_{\Sigma 3CSL}$ facet) is very low. The second close packed plane is $\{211\}_1$/$\{211\}_2$ or $(010)_{CSL}$ facet, the so-called asymmetric twin. The angle between facets $(100)_{CSL}$ and $(010)_{CSL}$ is 90°. The presence of such facets are well documented for Al, Au, $AuCu_3$, and Ge [62–65]. The typical rectangular twin plates with $(100)_{CSL}$ and $(010)_{CSL}$ facets can be seen, for example in Au thin films [19]. However, the twin plates in Cu and Ag are not rectangular. The end facet forms an angle of 82° with the $\{111\}_1$/$\{111\}_2$ or $(100)_{CSL}$ sides [58, 65]. TEM studies revealed that this 82° facet has so-called 9*R* structure forming a plate of bcc GB phase in the fcc matrix [66–68]. Such $(100)_{CSL}$ and 82° 9*R* facets on the Σ3 twin plate are clearly seen also in our samples in Fig. 2. EBSD measurements were performed in order to determine the deviation from the exact coincidence misorientation of Σ3 <110> tilt GB in Cu. The mea-

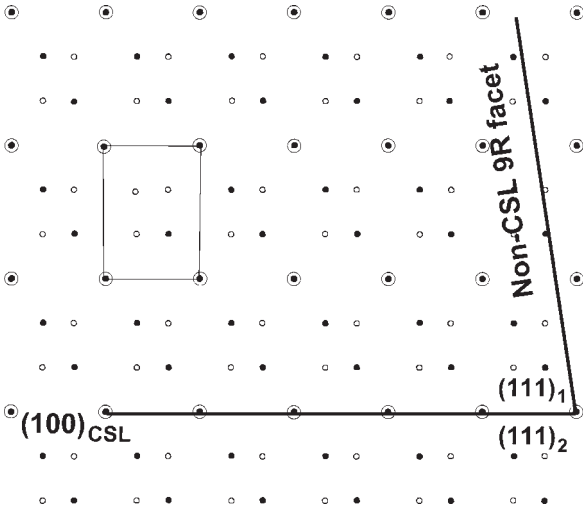

a)

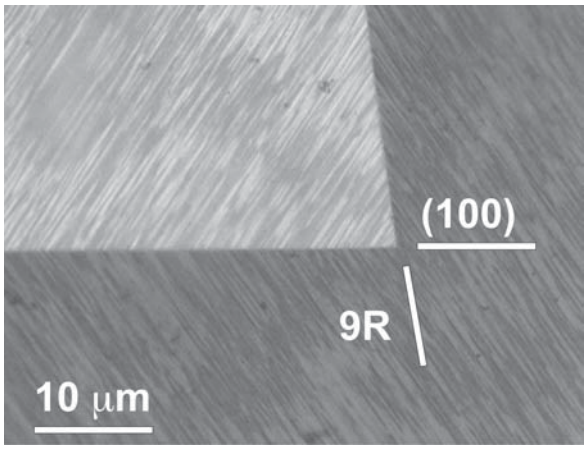

b)

Fig. 3. (a) Section of Σ3 CSL perpendicular to the {110} tilt axis with position of $(100)_{CSL}$ and 9R facets and (b) micrograph of intersection of $(100)_{CSL}$ and 9R facets, 1293K.

surements were made in different locations on the Cu sample. The maximal measured $\Delta\theta$ is only about 1°. The maximal reported $\Delta\theta$ for Σ3 is about 10-20° [51, 55]. At $\Delta\theta$ below 10° twin GBs still conserve their special structure and properties [51–57]. The resulting dependence of σ_{GB}/σ_{sur} ratio on deviation from the Σ3 coincidence misorientation $\Delta\theta$ for the 9*R* facet and $(100)_{CSL}$ facet have been shown in Fig. 4. The σ_{GB}/σ_{sur} ratio for the $(100)_{CSL}$ facet increases almost linearly from the very low value of 0.02 close to coincidence misorientation to 0.05. The σ_{GB}/σ_{sur} ratio for the 9*R* facet is much higher and fluctuates around value of 0.21.

In order to construct the 3-dimensional Wulff diagrams the data on inclination dependence of energy of Σ3 GBs in Cu obtained for the <110> and <211> tilt axes were used [62–64] together with data shown in Fig. 4. It was supposed that the energies for zero inclinations and zero deviation from the Σ3 coincidence misorientation are equal for all three cases. In Fig. 5 the 3-dimensional Wulff diagram is shown which is constructed for zero deviation from the Σ3 coincidence misorientation using the data [62–64]. The very low energy of coherent $(100)_{CSL}$ facets (thin central 'needle' on the Wulff plot) determine the platelet-like shape of twins in Cu (Fig. 1). It can be seen that with increasing $\Delta\theta$ the energy of symmetric twin increases, Wulff's diagram changes and becomes more 'spherical'. It means that by further increase of $\Delta\theta$ the transition from faceted to rough GB can occur, similar to that proceeding with increasing temperature. The metastable nature of the minor CSL facets is clearly seen in Figs. 5b and 6. The presence of the minor CSL facets in the sample reveal the existence of the energetic minima on the Wulff-Herring plot. It follows from Figs. 5b and 6, that these minima are not deep enough to allow the corresponding facets to be stable if the $(100)_{CSL}$ facets have low energy.

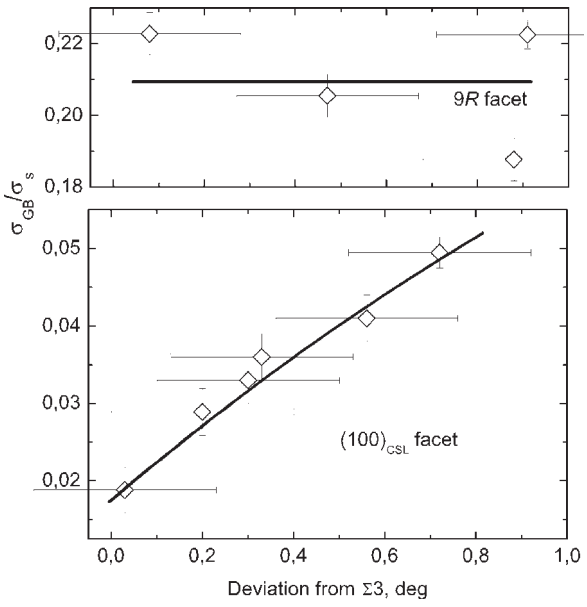

Fig. 4. Dependence of σ_{GB}/σ_{sur} ratio on deviation from the Σ3 coincidence misorientation for the 9*R* facet (top) and $(100)_{CSL}$ facet (bottom).

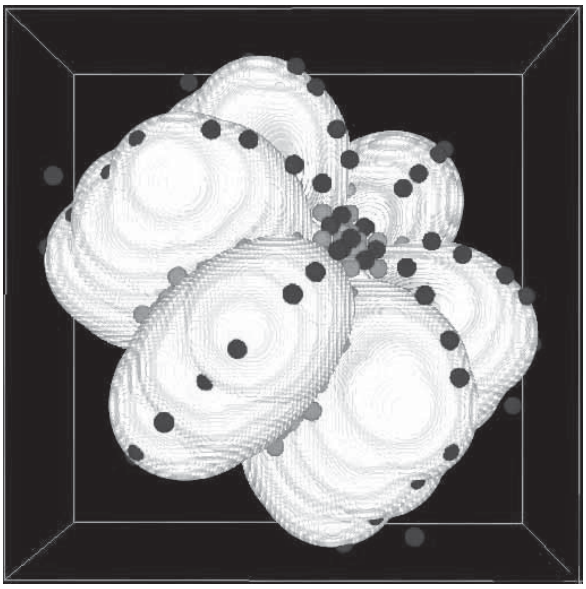

a)

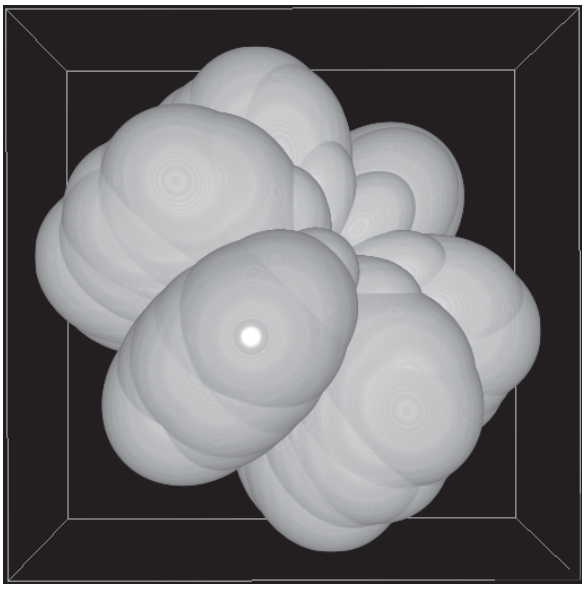

b)

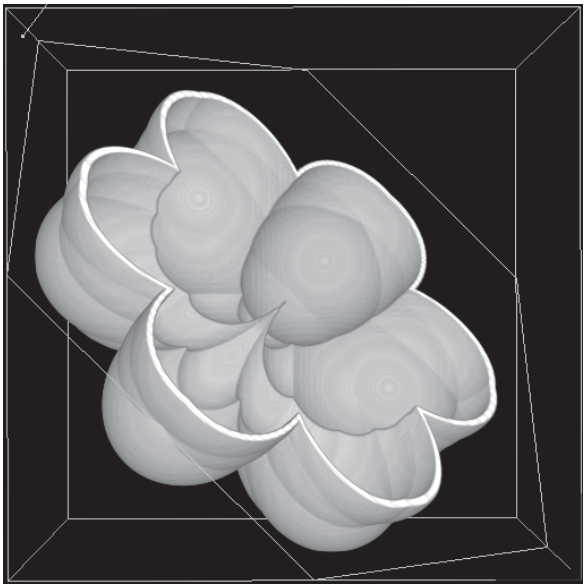

c)

Fig. 5. 3-dimensional Wulff plots for zero deviations from the Σ3 coincidence misorientation $\Delta\theta$ =0 (a) with experimental points from [62–64], (b) without experimental points, (c) section of the Wulff plot.

The observed $(100)_{CSL}$ / 82°9*R* edges of the twin plates are sharp. AFM reveals only minor rounding in the area with dimension less than 1 mm. It has been shown by Landau and Marchenko that the intersections of facets cannot be ideally sharp even well below the T_R [6, 69]. In other words, the roughening temperature T_R for $(100)_{CSL}$ and 9*R* facets is higher than the melting temperature T_m. By decreasing temperature new facets may appear in ECS of Σ3 GB [59]. All observed edges between facets are sharp. It means that the new facets appear not at the rough rounded GB like surface facets in Pb, Au or He [11–15] but at the sharp degenerated edges between existing facets. In other words, the true roughening temperature T_R is higher that the temperature T_{Rf} when a less densely packed CSL facet really appears in ECS. In our case the role of decreasing temperature plays the increasing $\Delta\theta$. By increase of $\Delta\theta$ the metastable minimum $(210)_{CSL}$ becomes stable. Such behaviour corresponds to the behaviour of areas of existence of special GBs [37, 43]. By decreasing temperature the areas of existence of special GBs become broader.

4. CONCLUSIONS

1. The cylindric tilt Σ3 GB in Cu bicrystal containing full spectrum of inclinations becomes fateted at 0.95 T_m.
2. The $(100)_{CSL}$, $(210)_{CSL}$, $(130)_{CSL}$ facets and non-CSL 82°9*R* facet are observed.
3. No rough edges between $(100)_{CSL}$ and 9*R* facets were observed. It means that T_m is lower than the roughening temperature for these facets in Cu.
4. The ratio between GB energy σ_{GB} and surface energy σ_{sur} was measured by atomic force microscopy using the GB thermal groove method. The influence of misorientation deviation $\Delta\theta = |\theta$

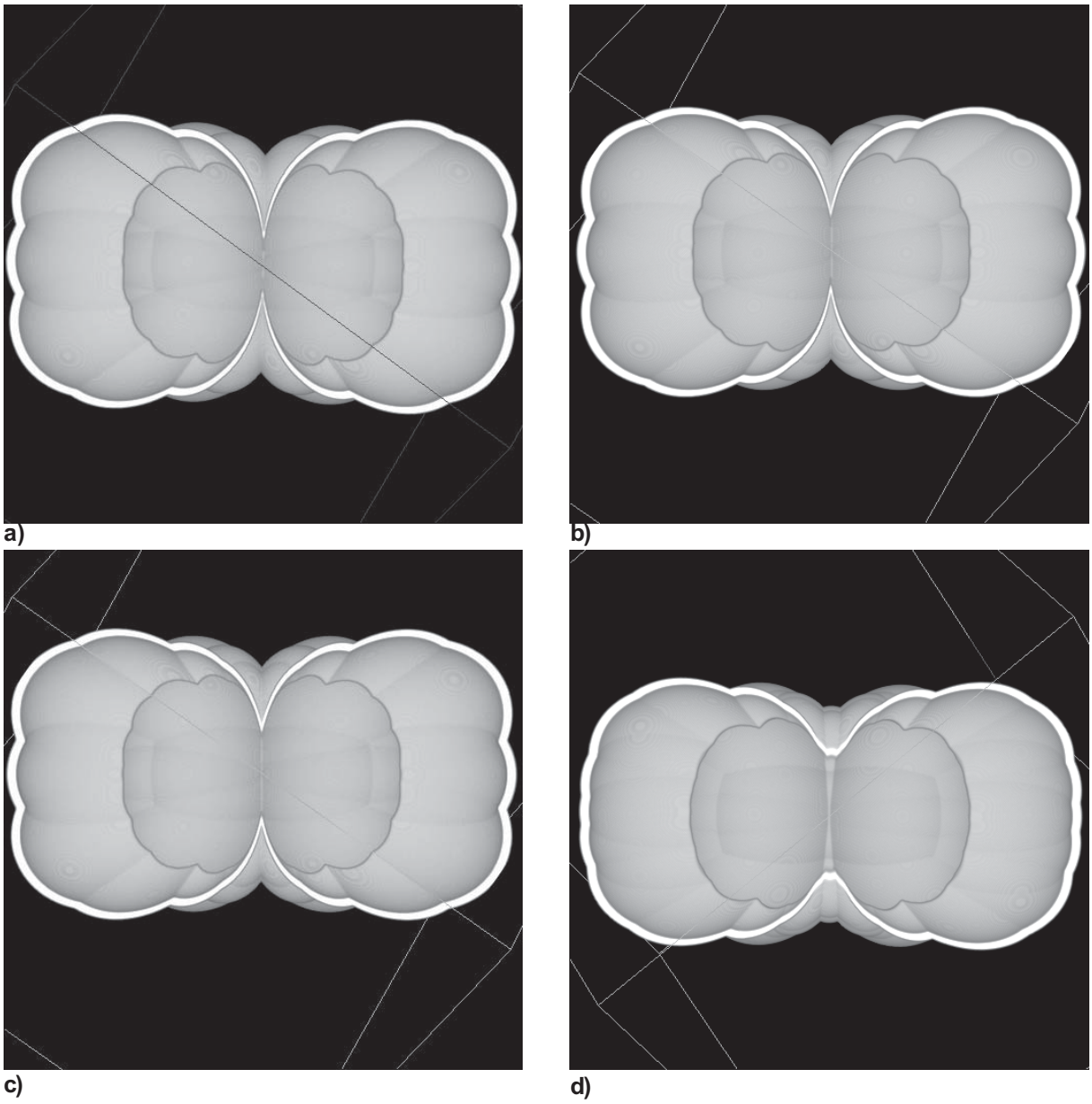

Fig. 6. The sections of 3-dimensional Wulff plots for different deviations from the Σ3 coincidence misorientation (a) $\Delta\theta$=0º, (b) $\Delta\theta$=0.4º, (c) $\Delta\theta$=0.8º and (d) $\Delta\theta$=0.98º.

$-\theta_\Sigma|$ from coincidence misorientation θ_Σ has been studied. The 3-dimensional Wulff-Herring diagrams were constructed using measured σ_{GB} / σ_{sur} values.

ACNOWLEDGEMENTS

Investigations were partly supported by the NATO Linkage grant (contract PST.CLG.979375), German Federal Ministry for Education and Research (conract RUS 04/014), INTAS (contract 03-51-3779) and Russian Foundation for Basic Research RFBR (contract 04-03-32800). Fruitful discussions with Profs. W. Gust, E. Mittemejer, E. Rabkin and Dr. E. Bischoff are acknowledged.

REFERENCES

[1] C. Herring // *Phys. Rev*. **82** (1951) 87.
[2] C. Rottman and M. Wortis // *Phys. Rev. B* **24** (1981) 6274; *Phys. Rev. B* **29** (1984) 328.
[3] G. Wulff // **Trudy Warsh. obsh. estestvoisp**. **6** (1894) 7, in Russian.

[4] G. Wulff // *Zeitschrift f. Krystallogr.* **34** (1901) 449, in German.
[5] A.F. Andreev // *Sov. Phys. JETP* **53** (1981) 1063 [*Zh. Eksp. Teor. Fiz.* **53** (1981) 2042].
[6] L.D. Landau and E.M. Lifshitz, *Statistical Physics* (Pergamon: Oxford, 1980), 3rd ed. revised by E.M. Lifshitz, L.P. Pitaevskii, Part 1.
[7] J. D. Weeks, In*: Ordering in Strongly Fluctuating Condensed Matter Systems,* ed. by T. Riste (Plenum: New York, 1980) p. 243.
[8] C. Rottman and M. Wortis // *Phys. Rep.* **103** (1984) 59.
[9] A.F. Andreev and A. Ya. Parshin // *Sov. Phys. JETP* **48** (1978) 763 [*Zh. Eksp. Teor. Fiz*. **75** (1978) 1511].
[10] K.O. Keshishev, A.Ya. Parshin and A.V. Babkin // *Sov. Phys. JETP* **53** (1981) 362 [*Zh. Eksp. Teor. Fiz*. **80** (1981) 716].
[11] J.C. Heyraud and J.J. Metois // *Acta Metal.* **28** (1980) 1789; *J. Cryst. Growth* **50** (1980) 571.
[12] J.C. Heyraud and J.J. Metois // *Surf. Sci*. **128** (1983) 334.
[13] R. Wagner, S.C. Steel, O.A. Andreeva, R. Jochemsen and G. Frossati // *Phys. Rev. Lett.* **76** (1996) 263.
[14] C. Rottman, M. Wortis, J.C. Heyraud and J.J. Metois // *Phys. Rev. Lett*. **52** (1984) 1009.
[15] Y. Carmi, S.G. Lipson and E. Polturak // *Phys. Rev. B* **36** (1987) 1894.
[16] V.L. Pokrovsky and A.L. Talapov // *Phys. Rev. Lett.* **42** (1979) 65.
[17] W.-C. Cheng and P. Wynblatt // *Surf. Sci.* **302** (1994) 185; **364** (1996) 109; **364** (1996) 417; *J. Cryst. Growth* **173** (1997) 513.
[18] M. Nowicki, C. Bombis, A. Emundts and H. P. Bonzel // *Phys. Rev. B* **67** (2003) 075405.
[19] D.C. Schlosser, L.K. Verheij, G. Rosenfeldand and G. Comsa // *Phys. Rev. Lett.* **82** (1999) 3843.
[20] G. Schulze, A. Icking-Konert, M. Giesen and H. Ibach // *Phys. Rev. Lett.* **83** (1999) 3880.
[21] M. Giesen, Ch. Steimer and H. Ibach // *Surf. Sci.* **471** (2001) 80.
[22] Ch. Steimer, M. Giesen, L. Verheijn and H. Ibach // *Phys. Rev.* B **64** (2001) 085416.
[23] A. Emundts, M. Nowicki and H.P. Bonzel // *Surf. Sci.* **496** (2002) L35.
[24] N.C. Bartelt and R.M. Tromp // *Phys. Rev.* B **54** (1996) 11731.
[25] H.J.W Zandvliet, S. van Dijken and B. Poelsema // *Phys. Rev.* B **53** (1996) 15429.
[26] S. Kodambaka, V Petrova, S.V. Khare, D.D. Johnson, I. Petrov and J.E. Greene // *Phys. Rev. Lett.* **88** (2002) 146101.
[27] S. Kodambaka, S.V. Khare, V Petrova, A. Vaillionis, I. Petrov and J.E. Greene // *Surf. Sci.* **513** (2002) 468.
[28] K. Arenhold, S. Surnev, H.P. Bonzel and P. Wynblatt // *Surf. Sci.* **424** (1999) 271.
[29] S.M. Bhattacharjee // *Phys. Rev. Lett.* **76** (1996) 4568.
[30] S. Song and S. G. J. Mochrie // *Phys. Rev. Lett.* **73** (1994) 995; Phys. Rev. B **51** (1995) 10068.
[31] D. Davidson and M. den Nijs // *Phys. Rev. Lett.* **84** (2000) 326.
[32] M.L. Kronberg and F.H. Wilson // *Trans. AIME* **185** (1949) 501.
[33] H. Grimmer // *Acta Cryst*. A **30** (1974) 680.
[34] H. Grimmer, W. Bollmann and D.T. Warrington // *Acta Cryst.* A **30** (1974) 197.
[35] A.N. Orlov, V.N. Perevesentsev and V.V. Rybin // *Sov. Phys. Sol. State* **17** (1975) 1662, in Russian.
[36] V.V. Rybin and V.N. Perevesentsev // *Sov. Phys. Sol. State* **17** (1975) 3188, in Russian.
[37] B. Straumal and L.S. Shvindlerman // *Acta Metal.* **33** (1985) 1735.
[38] B.B. Straumal, *Grain Boundary Phase Transitions* (Nauka publishers, Moscow, 2003), in Russian.
[39] C.W. Park, D.Y. Yoon, J.E. Blendell and C.A. Handwerker // *J. Amer. Ceramic Soc.* **86** (2003) 603.
[40] J.S. Choi and D.Y. Yoon // *ISIJ International* **41** (2001) 478.
[41] J.B. Koo and D.Y. Yoon // *Metal. Mater. Trans.* A **32** (2001) 469.
[42] S.B. Lee, D.Y. Yoon and M.F. Henry // *Acta Mater.* **48** (2000) 3071.
[43] E.L. Maksimova, L.S. Shvindlerman and B.B. Straumal // *Acta metall.* **36** (1988) 1573.
[44] K. Harada, S. Tsurekawa, T. Watanabe and G. Palumbo // *Scripta Mater.* **49** (2003) 367.
[45] L.C. Lim and R. Raj // *Acta metall.* **32** (1984) 1177.
[46] T. Watanabe, Y. Suzuki, S. Tanii and H. Oikawa // *Philos Mag Lett* **62** (1990) 9.
[47] T. Watanabe, K. -I. Arai, H. Terashima and H. Oikawa // *Solid State Phenom.* **37-38 (**1994) 317.
[48] J.K. Mackenzie and M.J.Thomson // *Biometrika* **44** (1957) 205.
[49] J.K. Mackenzie // *Biometrika* **45** (1958) 229.

[50] J.B. Koo, D.Y. Yoon, M.F. Henry // *Metal. Mater. Trans. A* **33** (2002) 3803.
[51] G. Dhalenne, M. Dechamps and A. Revcolevschi // *J. Am. Ceram.Soc.* **65** (1982) C11.
[52] D.J. Dingley and R.C. Pond // *Acta metall.* **27** (1979) 667.
[53] G. Hasson and C. Goux // *Scripta metall.* **5** (1971) 889.
[54] J.W. Matthews // *Scripta metall.* **11** (1977) 233.
[55] A. Otsuki and M. Mitsuno // *Trans. Jap. Inst. Met. Suppl.* **27** (1986) 789.
[56] T. Schober and R.W. Balluffi // *Phil. Mag. A.* **21** (1970) 109.
[57] T. Schober and D.H. Warrington // *phys. stat. sol. (a)* **6** (1971) 103.
[58] T. Muschik, W. Laub, M.W. Finnis and W. Gust // *Z. Metallk.* **84** (1993) 596.
[59] B.B. Straumal, S.A. Polyakov, E. Bischoff, W. Gust and E.J. Mittemeijer // *Interface Sci* **9** (2001) 287.
[60] J. Schölhammer, B. Baretzky, W. Gust, E. Mittemeijer and B. Straumal // *Interf. Sci.* **9** (2001) 43.
[61] J. Schoellhammer, L.-S. Chang, E. Rabkin, B. Baretzky, W. Gust and E.J. Mittemeijer // *Z. Metallkd*. **90** (1999) 687.
[62] W. Laub, A. Oswald, T. Muschik, W. Gust and R.A. Fournelle, In: *Solid–Solid Phase Transformations*, ed. by W.C. Johnson *et al.* (The Minerals, Metals & Materials Society: Warrendale, PA, 1994) p. 1115.
[63] A. Oswald, W. Laub, W. Gust and R.A. Fournelle, In: *Solid–Solid Phase Transformations,* ed. by W.C. Johnson *et al.* (The Minerals, Metals & Materials Society: Warrendale, PA, 1994) p. 1121.
[64] F. Ernst, M.W. Finnis, A. Koch, C. Schmidt, B. Straumal and W. Gust // *Z. Metallkd.* **87** (1996) 911.
[65] A. Barg, E. Rabkin and W. Gust // *Acta metall. mater.* **43** (1995) 4067.
[66] U. Wolf, F. Ernst, T. Muschik, M.W. Finnis and H.F. Fischmeister // *Phil. Mag. A* **66** (1992) 991.
[67] F. Ernst, M.W. Finnis, D. Hoffmann, T. Muschik, U. Schönberger and U. Wolf // *Phys. Rev. Lett.* **69** (1992) 620.
[68] D. Hofmann and M.W. Finnis // *Acta metall. mater.* **42** (1994) 3555.
[69] V.I. Marchenko // *Sov. Phys. JETP* **54** (1981) 605.